Analysis on the Deflection Angle of Columnar Dendrites of Continuous Casting Steel Billets Under the Influence of Mold Electromagnetic Stirring

XINCHENG WANG, SHENGQIAN WANG, LIFENG ZHANG,
SEETHARAMAN SRIDHAR, ALBERTO CONEJO, and XUEFENG LIU

In the current study, the deflection angle of columnar dendrites on the cross section of steel billets under mold electromagnetic stirring (M-EMS) was observed. A mathematical model was developed to define the effect of M-EMS on fluid flow and then to analyze the relationship between flow velocities and deflection angle. The model was validated using experimental data that was measured with a Tesla meter on magnetic intensity. By coupling the numerical results with the experimental data, it was possible to define a relationship between the velocities of the fluid with the deflection angle of high-carbon steel. The deflection angle of high-carbon steel reached maximum values from 18 to 23 deg for a velocity from 0.35 to 0.40 m/s. The deflection angles of low-carbon steel under different EM parameters were discussed. The deflection angle of low-carbon steel was increased as the magnetic intensity, EM force, and velocity of molten steel increased.

I.   INTRODUCTION

CONTINUOUS casting (CC) of steel is a complex process that involves heat transfer, fluid flow, and solidification, which in some cases occurs under an electromagnetic (EM) field.[1] EM fields are applied to achieve a better product quality and a higher productivity in the industry by generating the swirling flow.[2] The quality and property of continuous casting products are strongly related to the microstructure developed during solidification. The solidification microstructure can generally be categorized into a chilled layer zone, columnar zone, columnar-to-equiaxed transition (CET) zone, and equiaxed zone. The size of these zones is affected by many factors including superheat, casting speed, cooling rate, and EM fields.[3]

The application of EM field provides a considerable potential to control the fluid flow of the molten steel in the mold. Mold electromagnetic stirring (M-EMS) can enhance the area fraction of the CET in the billet compared to without M-EMS during solidification.[4] The frequency of M-EMS has little effect on the electromagnetic torque, but the current intensity has great influence. The equiaxed crystal ratio increases by 0.159 when increasing the torque from 230 to 400 cN cm.[5]

The normal growth direction of columnar dendrites is in the direction of extraction of heat in the mold. Three driving forces control crystal growth: thermal gradients, concentration gradients, and momentum gradients. A higher driving force around the tip of the columnar dendrite defines the direction of growth. Since the 1980s, deflection of columnar dendrite from its normal growth direction has frequently been observed in the presence of liquid flow in front of the solid–liquid interface during solidification.[6–13] The deflection angle was found to be the result of solute depletion in the upstream direction and higher solute concentration in the downstream direction due to convective flow around the tip of the columnar crystals.[12,14,15] In these conditions, the concentration gradient increases in the upstream direction. A deflection angle from 6 to 12 deg was reported during the solidification of an Al-Cu alloy due to an increase in liquid velocities from 0.001 to 0.02 m/s.

The information available on the deflection angle in steels is poor. Most of these results involve natural convection. Takahashi et al.[6] reported an increase in the deflection angle from 0 to 30 deg as the flow velocity increased from 0.1 to 0.4 m/s. Okano et al.[7] reported deflection angles from 10 to 30 deg and used these values to estimate the flow velocity. Esaka et al.[9] reported that the deflection angle increased from 15 to 20 deg as the carbon content increased from 0.01 to 0.1 pct, remaining constant at about 22 deg above this concentration. They also developed a mathematical model to predict the deflection angle, defined as the

XINCHENG WANG, Ph.D. Student, SHENGQIAN WANG, Postdoctoral Fellow, and LIFENG ZHANG, Professor, are with the Beijing Key Laboratory of Green Recycling and Extraction of Metals (GREM) and the School of Metallurgical and Ecological Engineering at the University of Science and Technology Beijing (USTB), Beijing 100083, China. Contact e-mail: wsqustb@126.com SEETHARAMAN SRIDHAR, RAEng/TATA Steel Chair and Director, is with the Advanced Steel Research Centre, WMG, University of Warwick, Coventry, CV47AL, U.K. ALBERTO CONEJO, Visiting Professor, is with the Morelia Technological Institute, Morelia 58120 México, and also with the University of Science and Technology Beijing (USTB). XUEFENG LIU, Professor, is with the School of Materials Science and Engineering at University of Science and Technology Beijing (USTB).

angle between the growth direction and the steepest concentration gradient. Natsume et al.[16] also reported an increase in the deflection angle as the velocity of the liquid increased with a maximum value of 14 deg at a velocity of 0.15 m/s.

The influence of M-EMS on many aspects of the continuous casting process has been investigated in the past.[2,4,5,10,17–22] However, only one previous research reported data on the deflection angle under the influence of M-EMS. In that work,[23] it is indicated that the deflection angle is effected by the solute and temperature gradients induced by fluid flow not by the EM force directly and 60 pct of the imposed electromagnetic force disappears due to the interaction of 3D flow, for example, from the submerged entry nozzle. In the current work, the deflection angle of the columnar crystals on the cross section of high-carbon and low-carbon steels under M-EMS was measured. In this paper, a mathematical model was developed to describe the EM force and velocity fields to elucidate the experimental observations of continuous casting billets that were from industry.

II. EXPERIMENTAL METHODOLOGY

Two kinds of continuous casting steel billets were used in this study. High-carbon steel GCr15 with 1 pct C and 1.4 to 1.65 pct Cr is one of the most commonly used high-chromium bearing steels, and low-carbon steel SAE8620H(s) with 0.2 pct C is a typical steel for gears. The solidification structure of one sample of high-carbon steel billet with a cross section of 220 mm × 300 mm and four samples of low-carbon steel with a cross section of 300 mm × 360 mm were analyzed in this work.

The continuous casting process parameters are listed in Table I. It should be noted that a M-EMS current of 450 amperes and a mold length of 800 mm was applied during the production of the high-carbon steel and a current of 220 amperes and a mold length of 734 mm was applied during the production of the low-carbon steel. The positions of M-EMS are shown in Figure 1. The chemical composition of the steel was analyzed using an Optical Emission Spectrometer Foundry-Master Xpert (manufactured by OBLF-Germany, model VeOS), and the results are shown in Table II. The samples were polished in preparation for the analysis of the solidification structure through macro etching. The polishing equipment (manufactured by Juhua-China, model JH-07C175) left a surface roughness of 0.6 to 0.8 μm. Macro etching was carried out using a hydrochloric acid solution 1:1 at 348 K (75 °C), for 2 hours. To obtain images of the solidification structure, a scanner was employed with an optical resolution of 1200 × 1200 dpi. The deflection angle of columnar dendrites was measured using the software Image-J, a Java-based image-processing program developed at the National Institutes of Health (NIH-USA). The deflection angle of columnar dendrites in a cross-sectional plane of the billet was measured along the lines of 10, 20, and 30 mm beneath the side surface. To compare deflection angles at different planes, further polishing in a section of a high-carbon billet was carried

Table I. Continuous Casting Process Parameters of High- and Low-Carbon Steels

Steel	Parameters	Value
High carbon steel	superheat	293 K (20 °C)
	casting speed	0.68 m/min
	solidus temperature	1608 K (1335 °C)
	liquidus temperature	1731 K (1458 °C)
	length of mold	800 mm
	working length of mold	700 mm
	cross-section of billet	300 × 220 mm²
Low carbon steel	superheat	299 K to 301 K (26 °C to 28 °C)
	casting speed	0.55 m/min
	solidus temperature	1738 K (1465 °C)
	liquidus temperature	1786 K (1513 °C)
	length of mold	704 mm
	working length of mold	634 mm
	cross-section of billet	360 × 300 mm²
	radius of continuous caster	12 m
	water flow rate at the mold	130 m³/h
	water temperature difference of the mold copper plate	280.9 K (7.9 °C)
	frequency of M-EMS	2.5 Hz
	current of M-EMS	450 A
	frequency of F-EMS	8.0 Hz
	current of F-EMS	750 A
	radius of continuous caster	12 m
	water flow rate at the mold	165 m³/h
	water temperature difference of the mold copper plate	275.6 K (2.6 °C)
	frequency of M-EMS	2.2 Hz
	current of M-EMS	220 A
	frequency of F-EMS	8.0 Hz
	current of F-EMS	150 A

out along the line of 20 mm, at progressive depths from 1 to 10 mm. The results on deflection angles are reported in Tables III, IV and VI.

The magnetic intensity in the mold was measured using a Tesla meter (Manufactured by Hengtong-China, model HT208). This model has a measuring range from 0 to 1000 mT. Measurements were made every 40 mm along the centerline of the mold from the top. These data were used to validate the mathematical model from this work.

III. MODEL FORMULATIONS

A. Assumptions of Simulation

To simplify the complexity of the actual operation and ensure reliable simulation results from the mathematical model, the following assumptions were made:

i. The stainless steel protective jacket and insulation materials of the EMS device as well as the cooling water jacket of the mold are all considered to be paramagnets.
ii. The electromagnetic phenomena is assumed to be a magneto quasi-static problem.
iii. The molten metal is considered to be a homogeneous phase, and its physical properties including density, viscosity, and conductivity are treated as constants.
iv. The effect of the melt flow on the electromagnetic field is ignored.
v. The molten metal is an incompressible fluid, and its flow is at steady state in the mold.
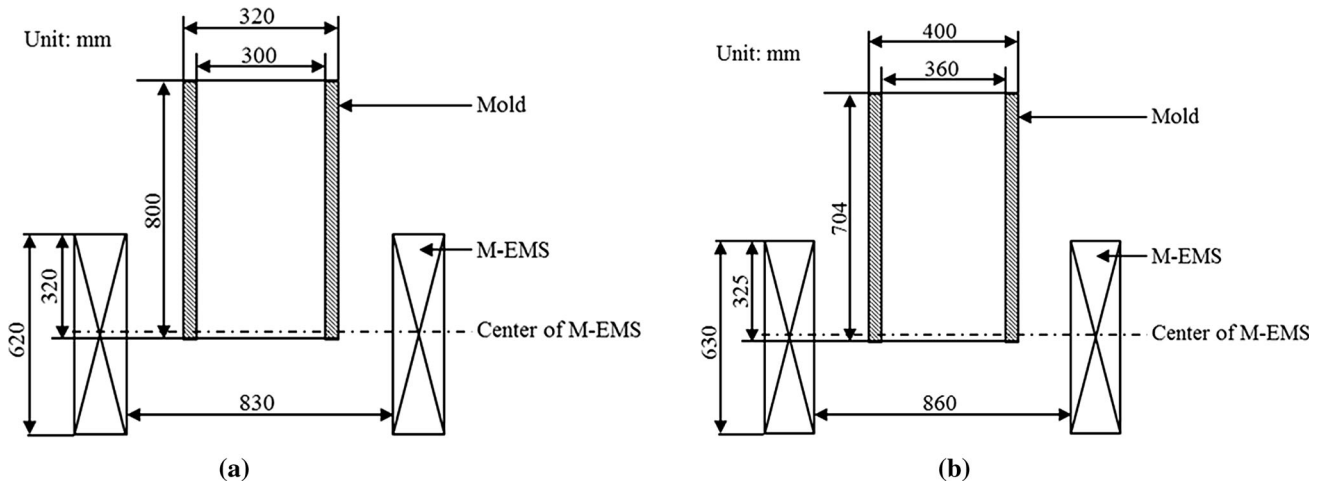vi. The solidification phenomenon is not calculated in the current model.

Fig. 1—Installation position of the M-EMS: (a) high-carbon steel and (b) low-carbon steel.

Table II. Chemical Composition of High- and Low-Carbon Steels (Weight Percent)

Steel	C	Si	Mn	P	S	Cr	Cu	Ni	Mo
high-carbon steel	0.97	0.21	0.33	0.013	0.007	1.47	0.01	0.017	0.0009
low-carbon steel	0.20	0.27	0.82	0.019	0.018	0.55	0.01	0.458	0.1780

Table III. Mean Value of the Measured Deflection Angle of High-Carbon Steel

	Mean Deflection Angle of Columnar Crystals		
	Distance Beneath Surface (mm)	Mean Deflection Angle at Different Positions (deg)	Mean Deflection Angle (deg)
From loose side	10	22.482	20.961
	20	21.029	
	30	19.372	
From fixed side	10	22.376	21.245
	20	21.519	
	30	19.841	
From left side	10	18.603	18.304
	20	18.644	
	30	17.665	
From right side	10	21.388	21.302
	20	21.216	

Table IV. Measurements on Deflection Angle of High-Carbon Steel at Different Depths and Along the Line Defined for 20 mm

Distance (mm)	1 mm	2 mm	3 mm	4 mm	5 mm	6 mm	7 mm	8 mm	9 mm	10 mm
55	−5.8	−5.0	5.1	6.3	3.8	3.7	9.9	5.0	−6.5	−5.1
60	16.7	25.6	10.2	17.7	23.5	26.1	11.6	26.1	22.0	5.1
65	13.2	18.4	18.3	14.3	25.6	20.7	18.4	14.6	23.1	12.3
70	17.0	17.7	7.1	11.6	14.6	21.4	18.9	22.4	26.6	17.3
75	21.2	19.9	12.5	24.4	21.4	24.1	22.5	24.0	25.0	20.3
80	20.2	23.6	16.9	27.1	24.4	26.6	24.2	25.5	27.1	24.5
85	23.9	25.6	24.2	25.0	26.1	27.1	23.0	27.1	27.1	25.0
90	23.3	25.6	25.1	25.1	25.0	25.6	24.9	24.6	17.3	27.1
95	24.2	29.5	26.0	28.1	26.1	27.1	25.4	25.6	25.6	26.6
100	27.5	28.5	28.4	28.4	26.1	25.0	25.4	25.1	26.1	27.1
105	27.5	27.6	28.4	27.1	25.6	26.1	27.7	26.1	29.0	26.1
110	27.5	29.0	27.2	26.6	27.1	27.6	28.2	27.1	28.5	25.6
115	27.5	29.5	29.1	27.6	28.1	28.1	28.2	27.1	28.0	23.5
120	27.5	29.5	29.7	29.4	29.6	27.6	27.7	27.6	28.1	24.5
125	27.5	29.5	29.7	29.4	26.0	25.0	28.2	26.1	28.1	25.6
130	27.5	29.5	29.7	29.4	26.1	26.1	26.0	25.0	29.5	28.7
135	27.5	29.5	29.7	29.4	28.5	27.6	28.2	27.1	29.6	27.6
140	27.5	29.5	29.7	29.4	28.6	29.5	27.1	28.1	29.0	28.9
145	27.5	29.5	29.7	29.4	30.0	28.5	29.3	30.3	30.0	29.6

B. Magnetic Field

The electric current density in the moving conducting fluid induced by the magnetic field is given by the Ohm's equation, and the EM field model is described by Maxwell's equations (Eqs. [1]–[4])[24]:

$$\nabla \times H = J + \frac{\partial D}{\partial t} \quad [1]$$

$$\nabla \times E = -\frac{\partial B}{\partial t} \quad [2]$$

$$\nabla \cdot B = 0 \quad [3]$$

$$\nabla \cdot D = \rho \quad [4]$$

where ∇ represents the del operator; H is the magnetic field strength (A/m); J is the current density (A/m^2); D is the electric flux density (C/m^2); E is the electric field strength (V/m); B is the magnetic flux density (T); ρ is the volume density of charge (C/m^3); and t is time (s).

Once the current distribution and the vector potential are known, the Lorentz force F can be calculated by Eq. [5]. The actual force can be expressed in a time-averaged form as Eq. [6][25]:

$$F = J \times B \quad [5]$$

$$F_{em} = \frac{1}{2}\text{Re}(J \times B^*) \quad [6]$$

where B^* is a conjugate complex number of B and $\text{Re}(J \times B^*)$ denotes the real part of a complex vector product $(J \times B^*)$.

C. Fluid Flow Field

In the current study, the three-dimensional fluid flow and EM field were coupled together. The Lorentz force was added to the momentum equation as a source term. The continuity equation, momentum equation, and energy equation are listed as follows:

Momentum equation:

$$\rho u \cdot \nabla \cdot u - \nabla(\mu_{\text{eff}} \cdot \nabla \cdot u) = -\nabla \cdot P + \rho g + F_{\text{em}} \quad [7]$$

where P is the pressure (Pa); F_{em} is the time-average Lorentz Force (N/m^3) as given by Eq. [6]; and μ_{eff} is the turbulence-adjusted effective viscosity (kg/m s), which is given by:

$$\mu_{\text{eff}} = \mu_l + \mu_t \quad [8]$$

where μ_l is laminar fluid viscosity (kg/m s) and μ_t turbulent fluid viscosity (kg/m s). The turbulent viscosity can be calculated using the k–ε turbulence model[26]:

$$\rho \frac{\partial k}{\partial t} + \rho u \cdot (\nabla \cdot k) = \nabla \cdot \left[\left(\mu + \frac{\mu_t}{\sigma_k}\right)\nabla k\right] + G_k + G_b - \rho \varepsilon \quad [9]$$

$$\rho \frac{\partial \varepsilon}{\partial t} + \rho u \cdot (\nabla \cdot \varepsilon) = \nabla \cdot \left[\left(\mu + \frac{\mu_t}{\sigma_\varepsilon}\right)\nabla \varepsilon\right] + C_1 \frac{\varepsilon}{k}(G_k + C_3 G_b) - C_2 \rho \frac{\varepsilon^2}{k} \quad [10]$$

where G_k is the generation of turbulence kinetic energy due to the mean velocity gradients (m^2/s^2); G_b is the generation of turbulence kinetic energy due to buoyancy (m^2/s^2); C_1, C_2, and C_3 are constants $C_1 = 1.44$,

$C_2 = 1.92$; and σ_k and σ_ε are the turbulent Prandtl numbers for k and ε, respectively, $\sigma_k = 1$ and $\sigma_\varepsilon = 1.3$.

D. Boundary Condition

Three-phase AC power is supplied to the coil windings for the calculation of the EM field in ANSYS 14.0. Each current phase is 120 deg, and the boundary condition for the EM field calculation is the flux-parallel boundary condition. For calculating the flow field in FLUENT, the inlet velocity of nozzle inlet can be calculated by Eq. [11]. The top of the mold is defined as a free surface, and the nozzle wall is defined as the no-slip surface. The outflow boundary condition is adopted for the outlet of computational domain:

$$V_{inlet} = \frac{V_c ab}{\rho_1 \pi r^2} \qquad [11]$$

where V_c is the casting speed (m/min); a is the length of mold (m); b is the width of mold (m); ρ_1 is the density of molten steel (kg/m^3); and r is the radius (m). The main dimensions and parameters for continuous casting parameters were listed in Table I.

E. Numerical Solution

The electromagnetic model and fluent of ANSYS 14.0 were used. The EM field was computed by the electromagnetic model, and then the magnetic data including real and imaginary part were obtained and written to a MAG file, which was invoked by the MHD model in FLUENT through software I/O between ANSYS and FLUENT (MHD)[27] that was developed by the current authors. The MHD model with the MAG file in FLUENT was used to calculate the fluid flow and EM field. The computational domains were defined using 390,000 cells in Figure 2. The convergence criterion for all variables was set to 10^{-5}. The SIMPLE scheme was used for the coupling between pressure and velocity. The spatial discretization schemes of the momentum, turbulent kinetic energy, and its dissipation rate were second-order upwind.
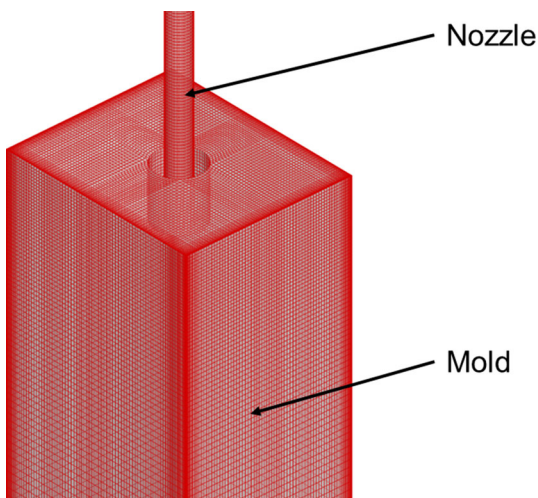

Fig. 2—Mesh system for flow field.

IV. RESULTS AND ANALYSIS

A. Deflection Angle of High-Carbon Steel

Figure 3 shows a general perspective of the solidification structure of the high-carbon steel billet, including the chilled zone, columnar zone, CET zone, and the equiaxed zone. Figure 4 shows a description of the deflection angle, including the upward and downward direction for dendritic crystal growth. The deflection angle in this way is given a positive value. The lines shown in Figure 4(b) schematically represent the deflection angle. Readings were carried out every 5 mm along the indicated lines. Figure 5(a) shows the solidification structure of the entire cross-sectional area evaluated in this work. Figure 5(b) shows in detail the measurements of deflection angle in the entire cross-sectional area. It can be observed that most angles are positive, except at the corners due to heat transfer in different directions. The deflection angles along the four faces of the billet are shown in Figure 6. The deflection angle increases from negative values at the corners to maximum values at the center of the billet. The corner is a transition zone in terms of deflection angle. At the corner, heat transfer is not unidirectional like that in the central part of the billet. The influence of heat extraction from two faces results in a negative deflection angle in the inner part of the corner. The magnitude of the deflection angle away from the corners is fairly uniform in all faces, reaching a value in the order of 18 to 23 deg. The deflection angle slightly decreases from the wall to the center of the billet. The average values at 10, 20, and 30 mm are 22, 21, and 19 deg, respectively. This result is an indication of higher flow velocities at the walls with respect to the center. It is also important to observe symmetrical results on deflection angles from the center to the two corners of each side of the billet.

Figure 7 compares the deflection angle of the columnar crystals 20 mm from the loose side surface at different surfaces, from 1 to 10 mm. The variation in the deflection angle at each surface shows a similar pattern. The relationship between the deflection angle and the distance from the narrow side can be expressed by the following expression, which is from the best fit simply:

$$\theta = 27.93 - 1331.49 e^{-0.074d} \qquad [12]$$

where θ is the deflection angle of columnar crystals (deg) and d is the distance from the narrow side (mm).

B. Numerical Modeling Results of High-Carbon Steel

1. Model validation

Figure 8 compares the magnetic intensity as a function of distance from the top of the mold between predictions and experimental results for the two sets of M-EMS, employing the electric parameters indicated in Table I. The magnetic intensity shows a Gaussian distribution with a maximum value of 0.07 T at about 900 mm for the first M-EMS and a maximum value of 0.05 T at about 850 mm for the second M-EMS. As it can be observed, the results from the model agree quite well with the experimental data.
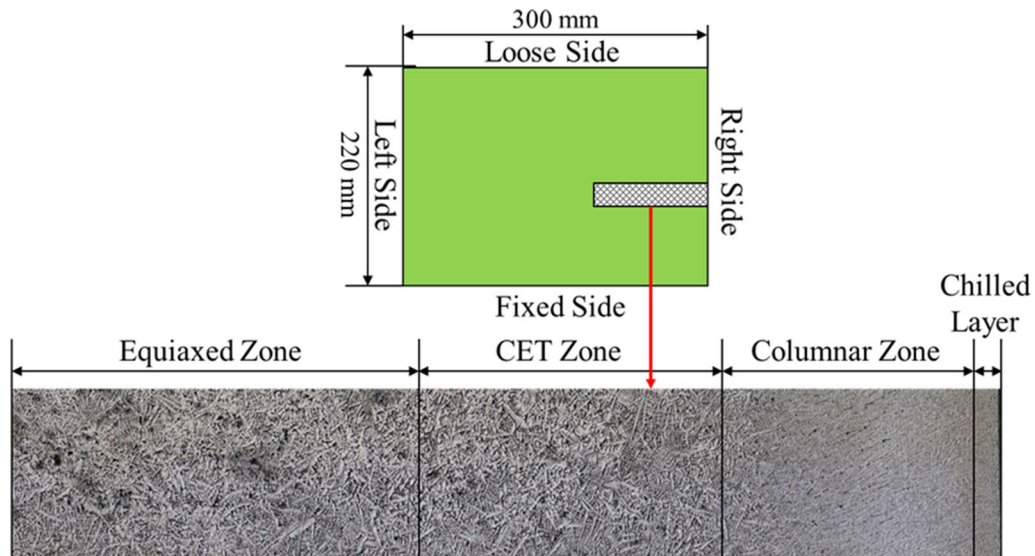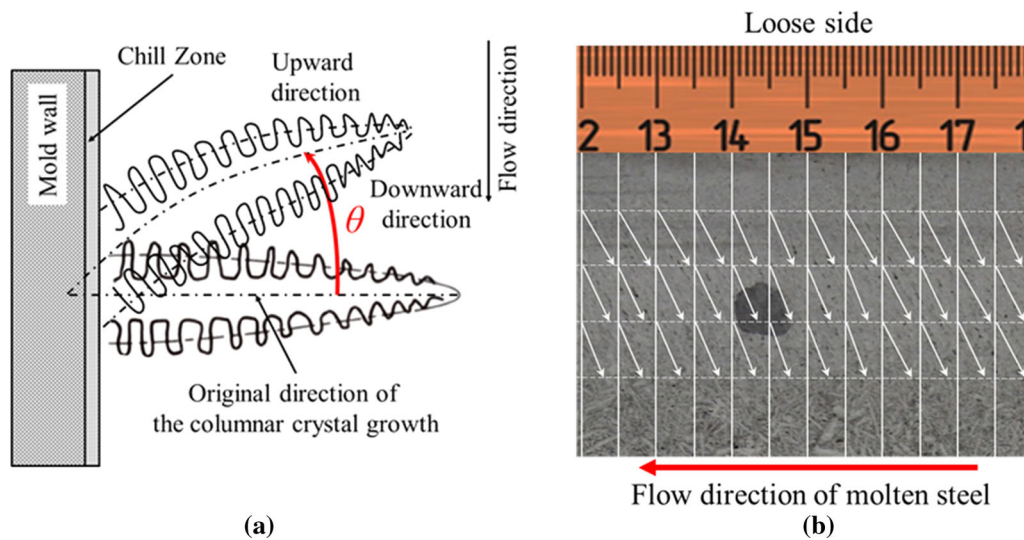
Fig. 3—Solidification structure of the billet.

(a)

(b)

Fig. 4—Example measurement of the deflection angle of the columnar crystals: (*a*) a description of the deflection angle and (*b*) actual measurement of the deflection angle.

2. *EM force and velocity fields*

The electromagnetic force and velocity of the liquid at the central plane of M-EMS is indicated in Figure 9. Figure 9(a) describes the electromagnetic force, indicating values from 1000 to 3500 N/m^3. It can be observed that from the rotational pattern of this force, which imparts a rotational flow recirculation of the liquid, as shown in Figure 9(b), the velocities range from 0.1 to 0.5 m/s.

The deflection angle is mainly affected by the tangential components of velocity since the fluid flow of molten steel has been changed by the EM force. The numerical results reported by the current model on the tangential EM force and tangential velocity along the same lines used to measure the deflection angle and a plane (central plane of M-EMS) located 10 mm above the bottom of the mold are shown in Figure 10. It is observed that the tangential force is maximum at the corners and minimum at the center of the billet walls due to the skin effect of alternating EM fields. The tangential force ranges from 1200 to 2800 N/m^3. On the contrary, the tangential velocity shows an opposite effect, and the maximum values are at the center of the billet walls and minimum values at the corners. The liquid reaches the corners of the mold and loses momentum due to impact with the walls, resulting in a decrease in velocities.

From Figure 11(a), it is observed that the tangential EM force has an opposite effect variation trend with the deflection angle. The angle decreased as the EM force increased. So the formation of the deflection angle of the columnar dendrite is not caused by the EM force directly but by the rotational flow recirculation induced by the EM force.
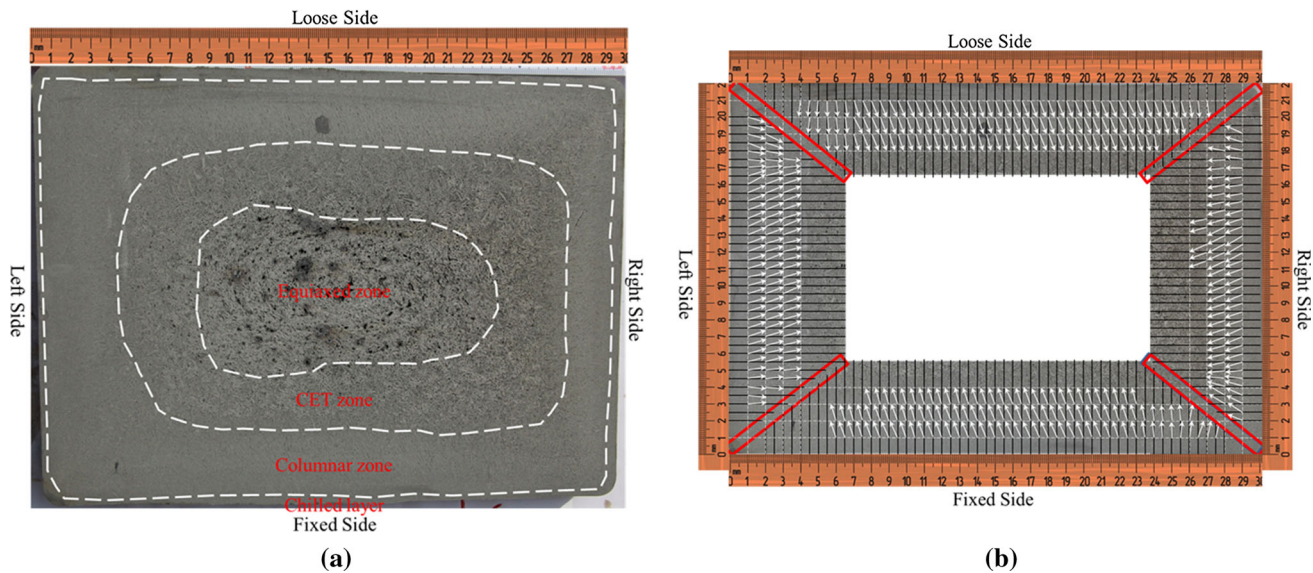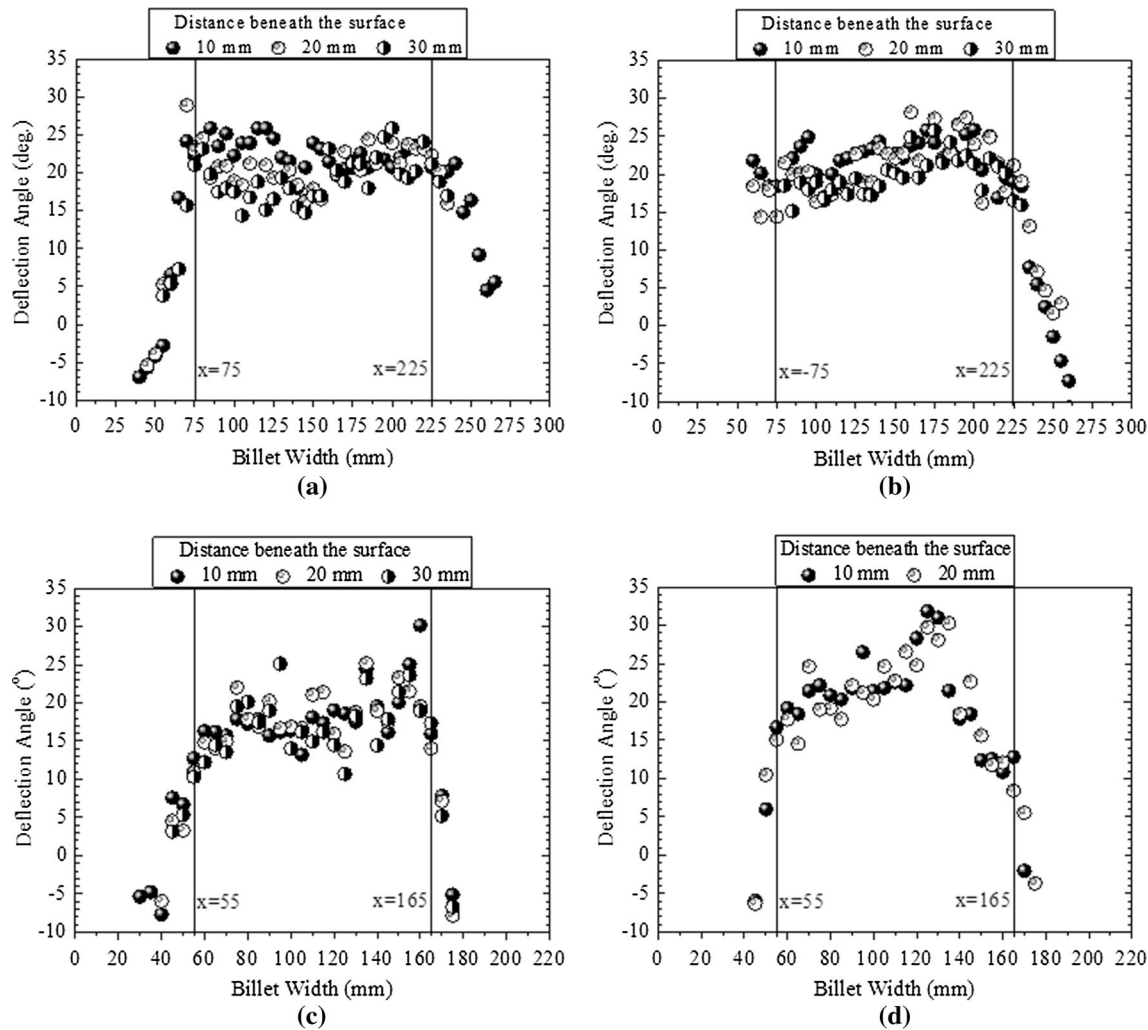
Fig. 5—Example measurement of the deflection angle of the columnar crystals: (*a*) a description of the deflection angle and (*b*) actual measurement of the deflection angle.

Fig. 6—Deflection angle of the columnar crystals for low carbon steel billet: (*a*) from loose side, (*b*) from fixed side, (*c*) from left side, and (*d*) from right side.
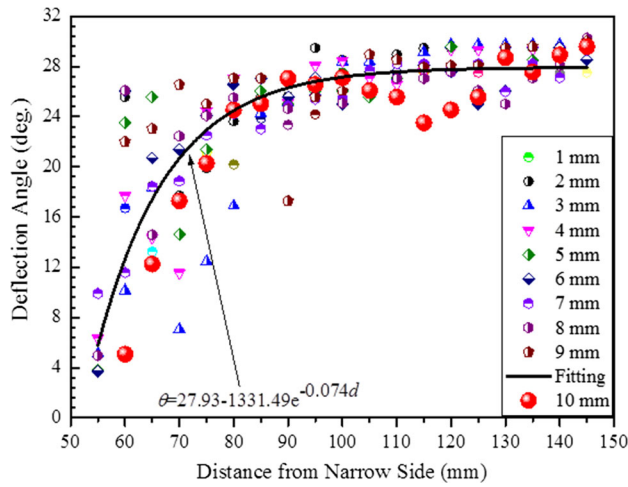
Fig. 7—Deflection angle of the columnar crystals beneath the loose side surface 20 mm at different etched depth surface for low-carbon steel.

By plotting the results on the tangential velocity reported by the numerical model against the deflection angle along the lines corresponding to the measured values, it is possible to obtain a relationship that defines the deflection angle in terms of the tangential velocity, as shown in Figure 11(b). The relationship obtained from this plot is as follows:

$$\left.\begin{array}{ll} \theta = -118.5 + 581.0V_T - 597.6V_T^2 & x = 10 \text{ mm} \\ \theta = -205.3 + 1129.6V_T - 1407.2V_T^2 & x = 20 \text{ mm} \\ \theta = -233.5 + 1474.5V_T - 2146.7V_T^2 & x = 30 \text{ mm} \end{array}\right\}$$

[13]

where V_T is the tangential velocity of liquid steel (m/s). The deflection angle of the columnar dendrites increases with the tangential velocity of the liquid. As the tangential velocity increases, the solute gradient and the temperature gradient between upstream and downstream directions around the dendritic tip also increases. When the velocity reaches a value of approximately
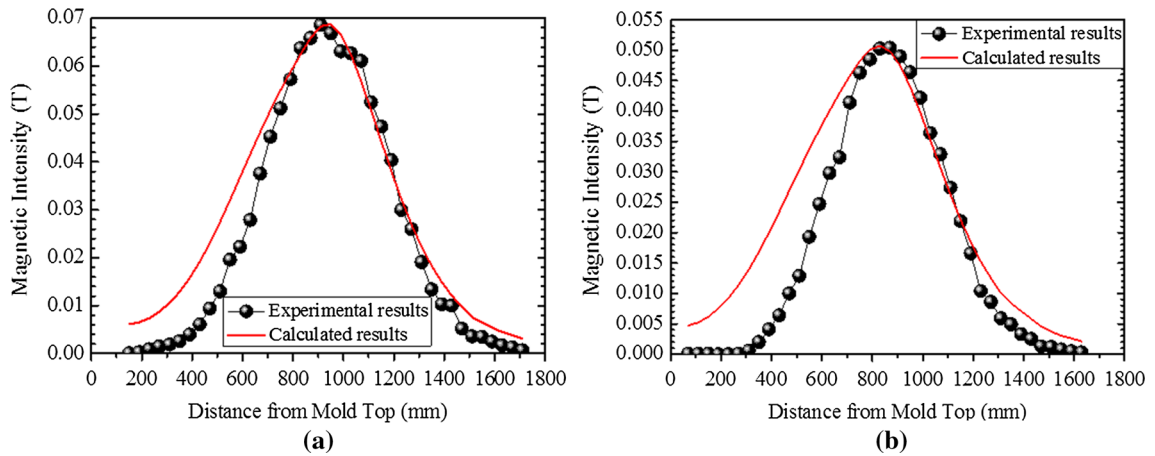
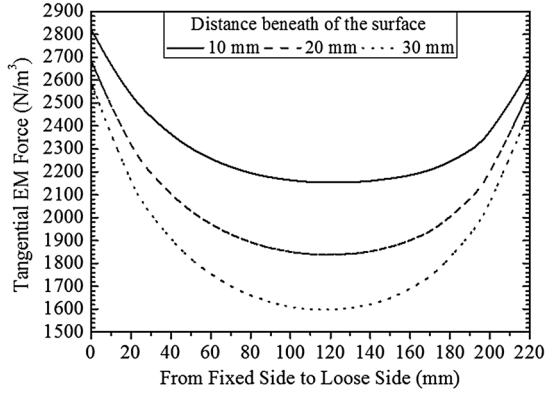Fig. 8—Experimental and calculated results of magnetic intensity: (*a*) high-carbon steel and (*b*) low-carbon steel.
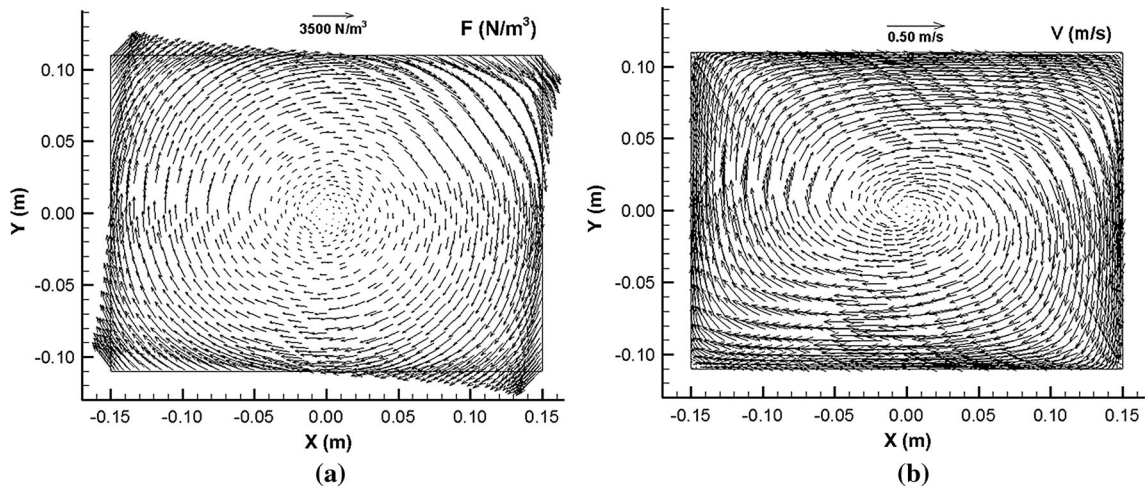
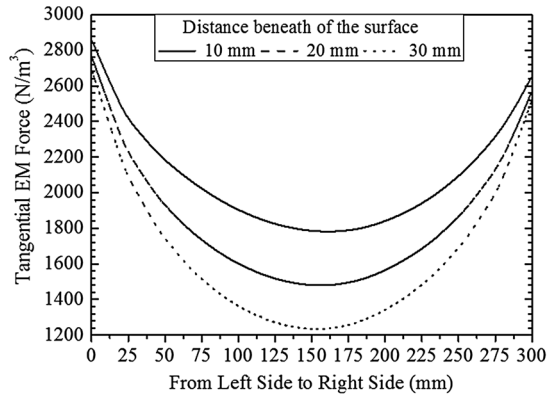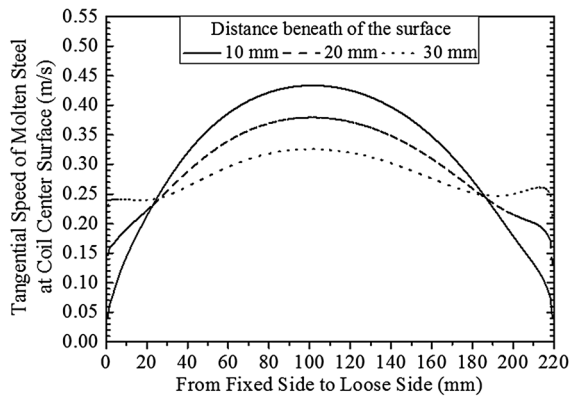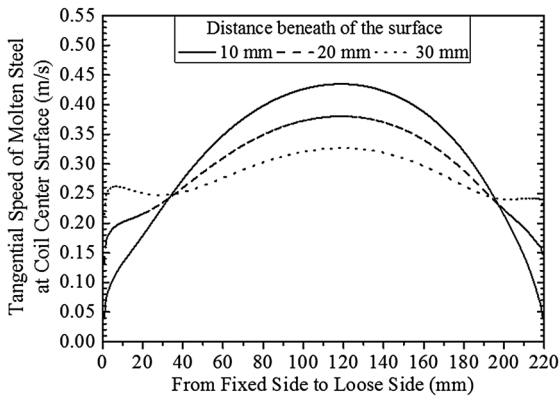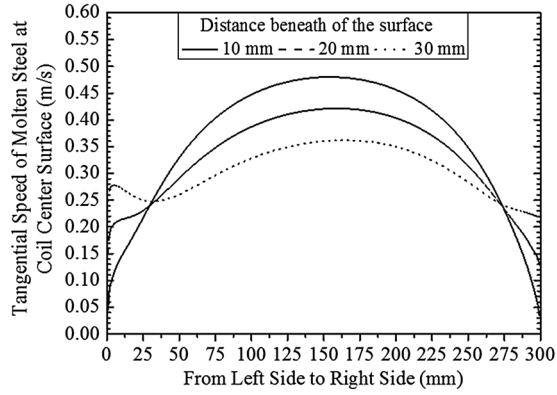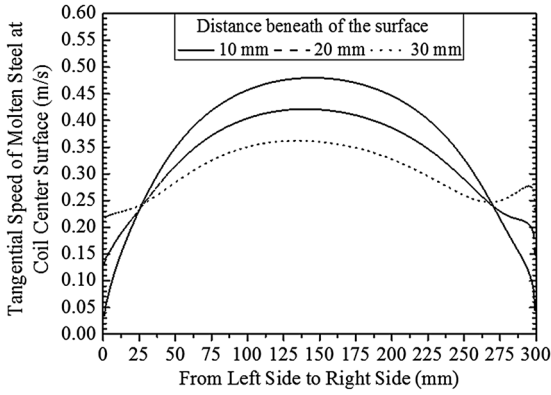Fig. 9—Calculated vector of tangential EM force and fluid flow velocity of the molten steel at central plane of M-EMS for high-carbon steel: (*a*) vector of tangential EM force and (*b*) fluid flow velocity of the molten steel.
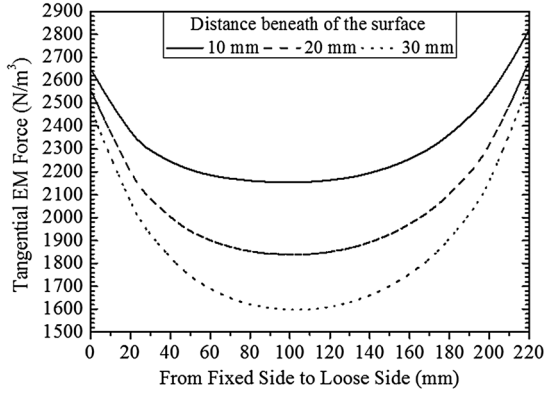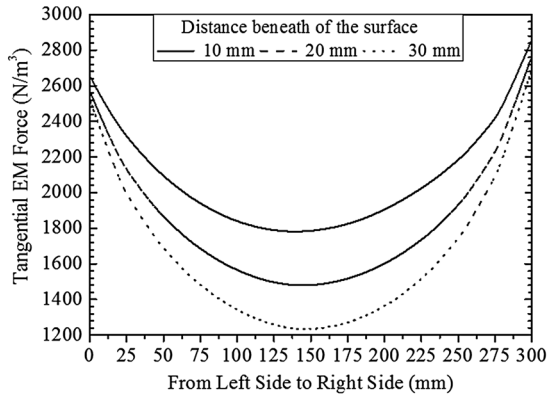
Fig. 10—Calculated results of EM force and flow speed of the molten steel for high-carbon steel: (*a*) EM force and (*b*) speed of molten steel.
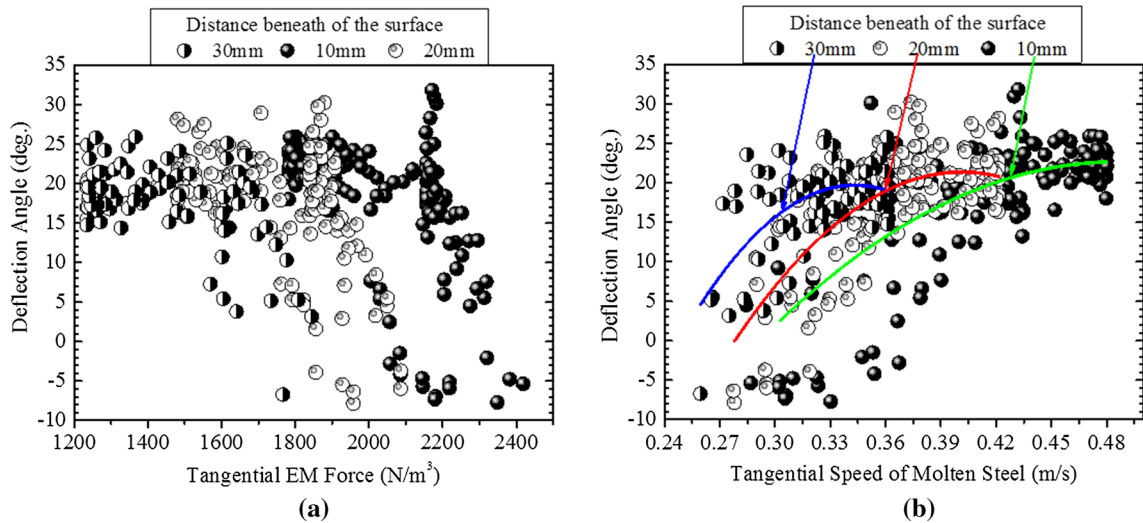
Fig. 11—Relationship between deflection angle and the calculated EM force and fluid flow velocity of the molten steel for high-carbon steel: (a) deflection angle and tangential EM force and (b) deflection angle and tangential velocity of molten steel.

Table V. Industrial Experimental Parameters of Low-Carbon Steel

No.	Superheat [K (°C)]	Casting Speed (m/min)	M-EMS (A/Hz)	F-EMS (A/Hz)
1	300 (27)	0.55	220/2.0	150/8.0
2	300 (27)	0.55	220/2.2	150/8.0
3	301 (28)	0.55	160/2.2	150/8.0
4	299 (26)	0.55	100/2.2	150/8.0

0.3 m/s, any further increase in velocity has a minor effect on the deflection angle as the solute and temperature gradients vary very little when the velocity exceeds this critical velocity (0.3 m/s) for this steel.

C. Deflection Angle Versus Current and Frequency for Low-Carbon Steel

1. Deflection angle with different EM parameters

The deflection angle of four low-carbon steel billets with the EM parameters listed in Table V was investigated using the method previously described for high-carbon steel billets. The difference of superheat for the four heats during the CC process was less than 275 K (2 °C), and the other parameters remained the same. The deflection angle of columnar dendrites was also observed on the cross section of the four low-carbon steel billets. The deflection angles along the four faces of the second billet are shown in Figure 12. The angles of the other three billets were also observed, and the average values of deflection angle in the central zone between two lines in Figure 12 were calculated and listed in Table VI. The deflection angle of low-carbon steel billets follows the same tendency as that for high-carbon steel billets. The magnitude of the deflection angle away from the corners is also fairly uniform in all faces, reaching a value in the order of 15 to 28 deg. The average values of the angle between the central zone with 220 A/2.0 Hz, 220 A/2.2 Hz, 160 A/2.2 Hz, and

100 A/2.2 Hz are 24.45, 24.85, 24.24, and 21.04 deg, respectively. When the frequency remains constant, there is an increase in the angle by increasing the current. When the current remains constant, there is an increase in the angle as the frequency increases. This result is an indication of higher stirring intensity in the molten steel induced by M-EMS with a larger deflection angle.

2. Magnetic intensity, EM force, and velocity fields with different EM parameters

A mathematical model to produce low-carbon steel billets involving M-EMS was also developed. In total, 64 cases with different EM parameters were simulated using the experimental parameters indicated in Table V. The average value of magnetic intensity (B_0), EM force (F), and speed of molten steel (V) at the central plane of M-EMS were reported by the mathematical model. The average value of B_0, F, and V is shown in Figure 13, and the values are listed in Table VII. Figure 13 shows the distribution of B_0, F, and V with a current ranging from 150 to 500 A and frequency ranging from 1 to 8 Hz. It is observed that the average value of magnetic intensity increases by increasing the current or decreasing the frequency; therefore, maximum values can be obtained with high current and low frequency. The average value of the EM force and the speed of molten steel both increase as frequency and current increase.
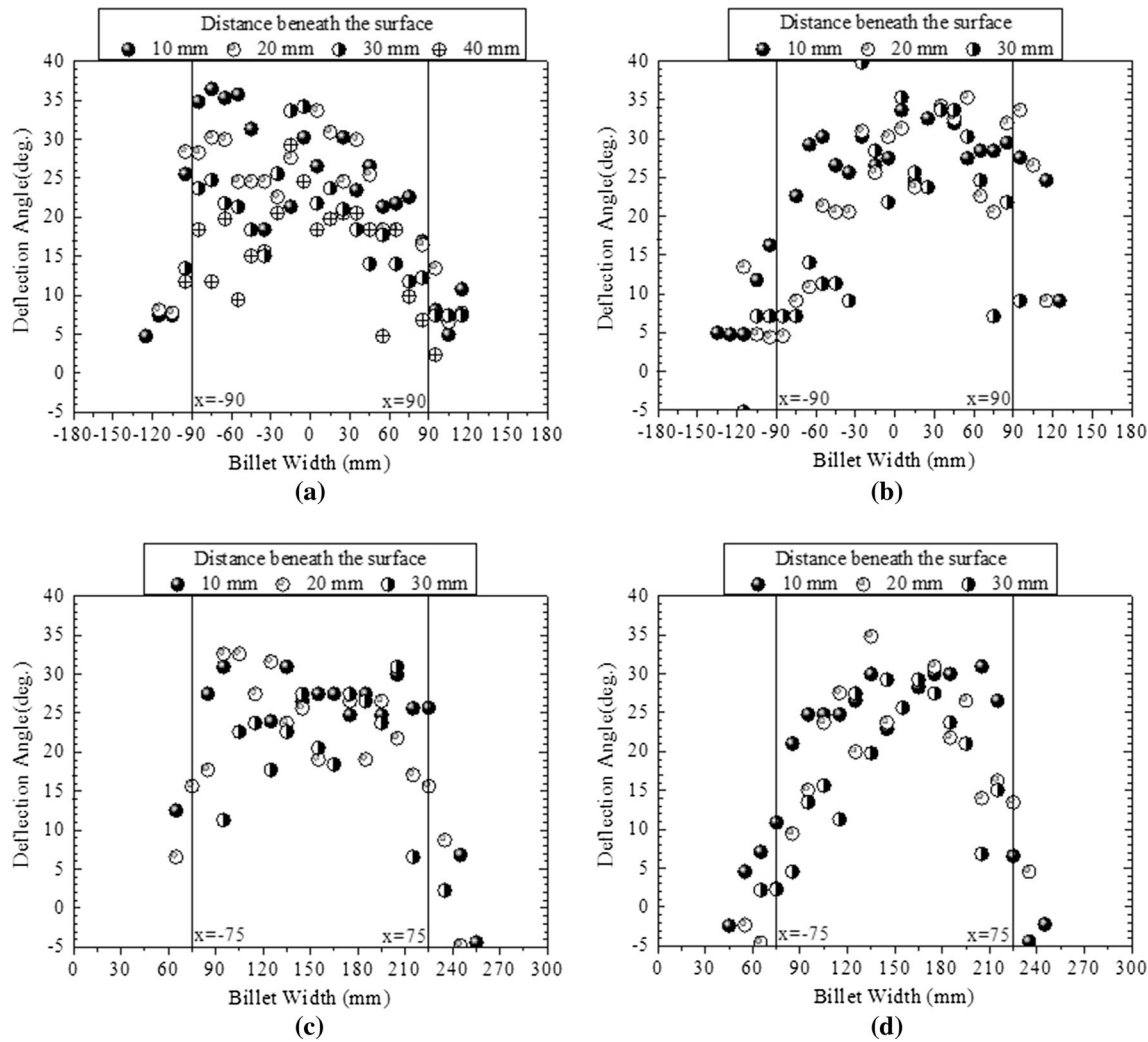
Fig. 12—Deflection angle of the columnar crystals of second low-carbon steel billet: (*a*) from loose side, (*b*) from fixed side, (*c*) from left side, and (*d*) from right side.

3. *Relationship between the angle and M-EMS*

The deflection angle is zero on the cross section of billet when there is no magnetic field in the mold. Figure 14 shows the relationship between the angle and the magnetic intensity, EM force, and velocity of molten steel. It can be seen that the angle increases as the magnetic intensity, EM force, and velocity of molten steel increase, but it reaches a maximum value when the magnetic intensity, EM force, and velocity of molten steel are larger than 0.033 T, 275 N/m^3, and 0.23 m/s, respectively. For this low-carbon steel, the solute and temperature gradients between upstream and downstream directions around the dendritic tip vary very little when the velocity exceeds 0.23 m/s. The relationship between these variables can be expressed by Eq. [14]. So, the optimal EM parameters can be obtained according to Figure 13 when the mean value of the angle was observed from the billet:

$$\left.\begin{array}{l} B_0 = 0.0237 - 0.0114\,\lg(24.691 - \theta) \\ F = 119.993 - 45.455\ln(24.677 - \theta) \\ V_T = 0.172 - 0.0226\ln(22.748 - \theta) \end{array}\right\} \quad [14]$$

The behavior of the columnar crystal is an important characteristic of the solidification structure, and it can reflect lots of information of the billet. From this discussion, the optimal parameters of the M-EMS can be obtained if the deflection angle of billets with different parameters (frequency and current) can be acquired after etching. In fact, the angle may relate to fluid flow, solute field, and temperature field, and the relationship between them will be discussed in a future article.

V. CONCLUSIONS

In the current article, the behavior of columnar crystals of bearing steel billets was observed under EMS and a three-dimensional model was developed to investigate the deflection angle of columnar crystals. The following conclusions were obtained:

1. The primary dendrite arm of the columnar crystal was off its original growing direction due to the

Table VI. Mean Value of the Measured Deflection Angle of Low-Carbon Steel Billets in the Central Zone

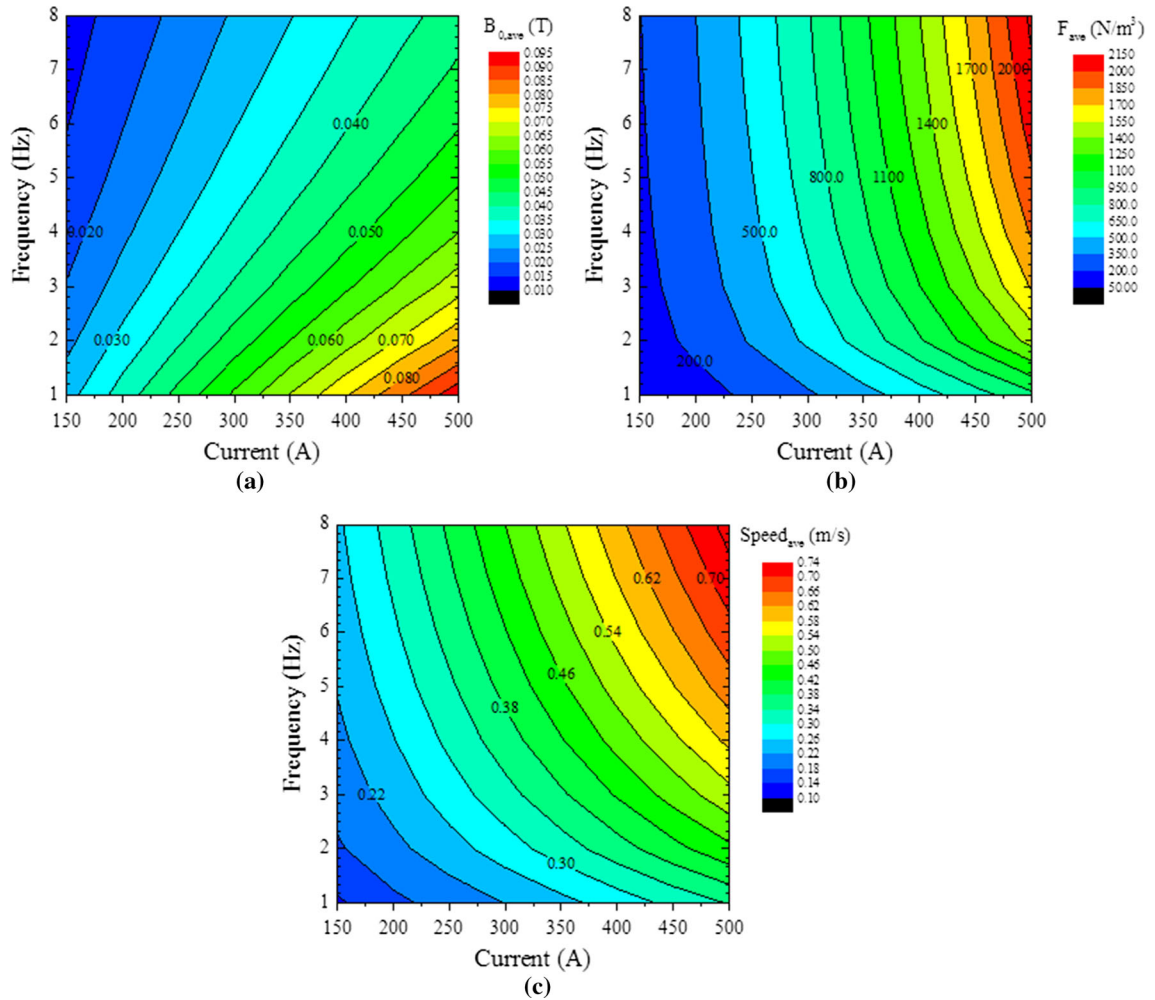| No.	M-EMS (A/Hz)	Mean Deflection Angle of Columnar Crystals Between the Central Zone at Each Side (Deg)				Mean Value (Deg)
		Loose Side	Fixed Side	Left Side	Right Side	
1	220/2.0	24.65	25.17	23.59	24.40	24.45
2	220/2.2	24.36	25.21	25.05	24.77	24.85
3	160/2.2	20.64	28.29	25.80	22.25	24.24
4	100/2.2	15.41	23.83	22.62	22.31	21.04

Fig. 13—Distribution of magnetic intensity, EM force, and speed of molten steel with different current and frequency at the central plane of M-EMS: (a) magnetic intensity, (b) EM force, and (c) speed of molten steel.

Table VII. Calculated Results of Industrial Experimental Condition

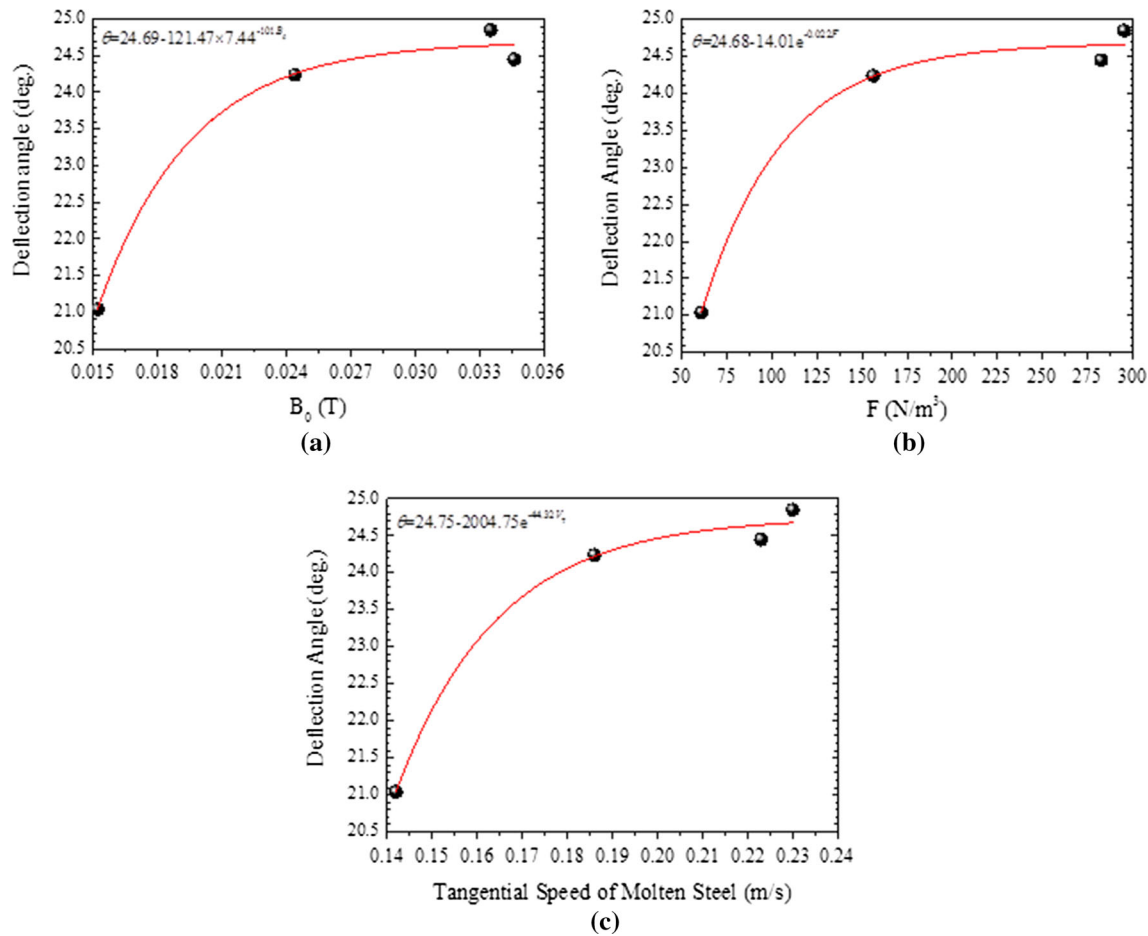| No.	M-EMS (A/Hz)	B_0 (T)	F (N/m^3)	V (m/s)
1	100/2.2	0.0152	60.99	0.142
2	160/2.2	0.0244	156.15	0.186
3	220/2.2	0.0335	295.19	0.230
4	220/2.0	0.0346	282.42	0.223

Fig. 14—Relationship between deflection angle and magnetic intensity, EM force, and speed of molten steel for low-carbon steel: (*a*) magnetic intensity, (*b*) EM force, and (*c*) speed of molten steel.

rotating molten steel flow under the action of the EM force produced by M-EMS; the deflection angle of the columnar crystal was largest at the middle width and the middle thickness of the billet and smallest at the corner of the billet.

2. The deflection angle of high-carbon steel reached maximum values from 18 to 23 deg for a velocity from 0.35 to 0.4 m/s. Any further increase in velocity had minor changes on the deflection angle.

3. Higher stirring intensity in the molten steel induced by M-EMS increases the deflection angle. The deflection angle of low-carbon steel is increased as the magnetic intensity, EM force, and velocity of molten steel is also increased and reaches a maximum value of 25 deg when their values are larger than 0.033 T, 275 N/m^3, and 0.23 m/s, respectively.

REFERENCES

1. B.G. Thomas: *Modeling for Casting and Solidification Processings*, 2001, vol. 15, pp. 499–540.
2. B. Ren, D. Chen, H. Wang, and M. Long: *Steel Res. Int.*, 2015, vol. 86 (9), pp. 1104–15.
3. M. Flemings: *Metall. Trans.*, 1974, vol. 5 (10), pp. 2121–34.
4. B. Wang, Z. Yang, X. Zhang, Y. Wang, C. Nie, Q. Liu, and H. Dong: *Metalurgija*, 2015, vol. 54 (2), pp. 327–30.
5. C. Jing, X. Wang, and M. Jiang: *Steel Res. Int.*, 2011, vol. 82 (10), pp. 1173–79.
6. T. Takahashi, K. Ichikawa, M. Kudou, and K. Shimahara: *Tetsu-to-Hagane*, 1975, vol. 61 (9), pp. 2198–213.
7. S. Okano, T. Nishimura, H. Ooi, and T. Chino: *Tetsu-to-Hagane*, 1975, vol. 61 (14), pp. 2982–90.
8. K. Murakami, T. Fujiyama, A. Koike, and T. Okamoto: *Acta Metall.*, 1983, vol. 31 (9), pp. 1425–32.
9. H. Esaka, F. Suter, and S. Ogibayashi: *ISIJ Int.*, 1996, vol. 36 (10), pp. 1264–72.
10. M. Bridge and G. Rogers: *Metall. Trans. B*, 1984, vol. 15 (3), pp. 581–89.

11. Y. Miyata: *ISIJ Int.*, 1995, vol. 35 (6), pp. 600–03.
12. S.Y. Lee, S.M. Lee, and C. Hong: *ISIJ Int.*, 2000, vol. 40 (1), pp. 48–57.
13. S. Park, H. Esaka, and K. Shinozuka: *J. Jpn. Inst. Metal.*, 2012, vol. 76 (3), pp. 197–202.
14. H. Esaka, T. Taenaka, H. Ohishi, S. Mizoguchi, and H. Kajioka: *J. Jpn. Soc. Microgravity App.*, 1989, vol. 6, pp. 20–25.
15. W.D. Griffiths and D.G. McCartney: *Mater. Sci. Eng. A*, 1996, vol. 216 (1–2), pp. 47–60.
16. Y. Natsume, K. Ohsasa, and T. Narita: *Mater. Trans.*, 2002, vol. 43 (9), pp. 2228–34.
17. P. Sahoo, A. Kumar, J. Halder, and M. Raj: *ISIJ Int.*, 2009, vol. 49 (4), pp. 521–28.
18. S. Zhou: *Metall. Int.*, 2013, vol. 18 (10), pp. 19–22.
19. H. Yu and M. Zhu: *Acta Metall. Sin.*, 2009, vol. 22 (6), pp. 461–67.
20. E. Wang, E. Jiang, G. Zhan, A. Deng, and J. He: *Mater. Sci. Forum*, 2012, vols. 706–709, pp. 2480–83.
21. H. Sun and J. Zhang: *Metall. Mater. Trans. B*, 2014, vol. 45B, pp. 1133–49.
22. S. Luo, M. Zhu, and S. Louhenkilpi: *ISIJ Int.*, 2012, vol. 52 (5), pp. 823–30.
23. H. Esaka, T. Toh, H. Harada, E. Takeuchi, and K. Fujisaki: *Tetsu-to-Hagane*, 2000, vol. 86 (4), pp. 247–51.
24. K. Wang, S. Chandrasekar, and H. Yang: *J. Mater. Eng. Perform.*, 1992, vol. 1 (1), pp. 97–112.
25. B. Zhang, Z. Ren, and J. Wu: *Trans. Nonferr. Metal. Soc. China*, 2006, vol. 16 (1), pp. 33–38.
26. S. Wang, L. Zhang, Y. Tian, Y. Li, and H. Ling: *Metall. Mater. Trans. B*, 2014, vol. 45B, pp. 1915–35.
27. L. Zhang and Y. Li: *Chinese Softw., No. 2013SR063168,* 2013.